

1 **Three western pacific typhoons strengthened fire weather in the recent conflagration**
2 **in northwest U.S.**

3
4 **S.-Y. Simon Wang¹, Jacob Stuivenvolt Allen¹, Matthew D. LaPlante^{1,2}, and Jin-Ho Yoon³**

5 ¹Department of Plants, Soils and Climate, Utah State University, Logan, UT, USA

6 ²Department of Journalism and Communication, Utah State University, Logan, UT, USA

7 ³School of Earth Sciences and Environmental Engineering, Gwangju Institute of Science and
8 Technology, Gwangju, South Korea

9 Corresponding author: Simon Wang (simon.wang@usu.edu)

10
11
12 **Key Points:**

- 13 • Anomalies of Rossby wave activity that began with recurring typhoons in the west
14 Pacific heightened extreme weather events in North America.
- 15 • In observational and forecast data, these typhoons have exacerbated fire weather
16 conditions through their impact to the jet-stream.
- 17 • Amplification of the trans-Pacific wave train led to a heatwave, strong winds and
18 associated fires in western U.S.
19

20 **Abstract**

21 A heatwave and fire outbreak in the western United States in early September of 2020 resulted
22 from an atmospheric wave train that spanned the Pacific Ocean basin. Days before the
23 atmospheric waves developed in the U.S., three western Pacific tropical cyclones underwent an
24 extratropical transition within an unprecedentedly short span of 12 days. Using a climate
25 diagnostic approach and historical forecast data from the Global Ensemble Forecast System
26 (GEFS), it was found that the amplitude of the atmospheric waves accompanying the western
27 U.S. fire weather would have been reduced if not for the influence of these cyclones. Together,
28 the recurving typhoons provided a significant source of Rossby wave activity toward North
29 America—amplifying the ridge over the U.S. west coast while deepening the trough in central
30 Canada. This anomalous circulation was a precursor to the severe frontal system that caused
31 extreme winds in western Oregon—starting and rapidly spreading fire.

32

33 **Plain Language Summary**

34 The weather pattern accompanying the heatwave in California and rapidly spreading fires in
35 Oregon in early September 2020 can be traced back to an unexpected source: typhoons in the
36 western Pacific. Three typhoons ran into the Korean Peninsula within two weeks leading up to
37 the heatwave and fire events. Together, Typhoon Bavi, Typhoon Maysak and Typhoon Haishe
38 contained substantial energy to perturb the jet-stream—creating a rippling atmospheric wave
39 train that had a pronounced effect on the hot-dry weather of western U.S. This study uses
40 forecast models and weather observations to show that these typhoons amplified areas of high
41 pressure and low pressure in North America leading to the intense winds which rapidly spread
42 fire in Oregon and Washington. While the impacts of climate change on these events were not
43 evaluated in this study, the implication is that the effect of weather extremes is not always
44 limited to the region in which those extremes occur.

45

46

47 **1 Introduction**

48 The unprecedented Oregon wildfires that have intensified rapidly on September 7, 2020,
49 have burned over 1 million acres and killed 23 people (as of 09/20/20), with about 500,000
50 people evacuated. The remarkable spread of fires occurred in association with an extreme wind
51 event that brought 25 to 50 mph winds to western Oregon (<https://wildfiretoday.com/>). This wind
52 event, which lasted through September 8, 2020, (Figure 1a) was caused by a powerful frontal
53 system that formed an unseasonably strong east-west pressure gradient, accompanied by an
54 amplified atmospheric ridge to its west. This amplified ridge was also blamed for a California
55 heatwave in the days before the fires (<https://www.npr.org/>). Together, the heat-trapping western
56 ridge and the front-producing eastern trough formed a quasi-stationary wave over North
57 America, one that had its origins in the western North Pacific (the evolution of this circulation
58 can be viewed at <http://tinyurl.com/TyphoonsToHeatWave>). Days before, the western North
59 Pacific saw three strong tropical cyclones that passed through the Korean Peninsula in rapid
60 succession: Typhoon Bavi (which reached Korea on August 26), Typhoon Maysak (which
61 reached Korea on September 2), and Typhoon Haishen (which reached Korea and Japan on
62 September 6). All three typhoons had maximum sustained wind speeds greater than 118 km/h
63 (74 mph) and all of them recurved and went through an extratropical transition. It was the first
64 time on record that Korea had been hit by three consecutive typhoons within two weeks, and
65 each typhoon was responsible for releasing Rossby wave energy into the midlatitude jet stream.

66 The meteorological community has known that as a typhoon recurves and undergoes
67 extratropical transition [*Jones et al.*, 2003], its interaction with the jet stream can perturb the
68 extratropical flow and trigger high-impact weather events far downstream (e.g., [*Agustí-
69 Panareda et al.*, 2005; *Harr and Dea*, 2009; *Hodyss and Hendricks*, 2010; *Namias*, 1963;
70 *Pantillon et al.*, 2013]). As shown in Figure 2a, *Archambault et al.* [2013] portrayed how a
71 recurving typhoon in the western North Pacific can amplify a high-latitude ridge over western
72 North America and an early season cold-air outbreak over the central United States. Generally a
73 recurving typhoon is steered ahead of a trough and contributes to wave amplification to the east
74 and jet stream intensification to the north. Extratropical cyclogenesis is then enhanced in
75 conjunction with Rossby wave dispersion, which amplifies a downstream ridge over western
76 North America. The amplified ridge provides dynamic forcing for a cold-air outbreak east of the
77 Rocky Mountains along with a baroclinic/low-pressure trough [*Archambault et al.*, 2013]. This
78 situation bears striking resemblance to what has transpired during early September 2020, but the
79 extent to which *three* recurving typhoons interacting with the extratropical flows in East Asia
80 contributed to the remarkable North American circulation anomaly is unclear. This study aims to
81 examine the role of the three consecutive typhoons, an unprecedented event of its own, in the
82 record heat and wind events in the West Coast.

83

84 **2 Data**

85 To evaluate the impact of western Pacific tropical cyclones (typhoons) on the recent
86 western U.S. heatwave and fire outbreak, this study used archived forecast data from the
87 National Centers for Environmental Prediction (NCEP) Global Ensemble Forecast System
88 (GEFS). The GEFS is produced four times daily with forecast times out to 16 days after the
89 initialization time. Twenty-one ensemble members at 1° resolution are run in each initialization,
90 with perturbations in the initial conditions gathered from the operational hybrid Global Data

91 Assimilation System 80-member Ensemble Kalman Filter [Whitaker *et al.*, 2008]. GEFS's
92 initializations with observed tropical storms use a tropical storm relocation technique to adjust
93 the model's central storm location to more accurately represent observations and offer more
94 accurate possibilities for tropical cyclone evolution due to initial conditions perturbations [Zhou
95 *et al.*, 2016]. We adopted the historical forecast data that were initialized from 00z August 23 (as
96 far back as the dataset goes) through 18z August 30, 2020 (to provide enough spread for
97 different scenarios). For any given day in September (e.g., 12Z 9/1), the forecast data consist of 4
98 $\times 8 \times 21 = 672$ members for the analysis. For observational data analysis, we used the 6-h NCEP-
99 NCAR Reanalysis with a 2.5° spatial resolution from 1948 to 2020 [Kalnay *et al.*, 1996].

100 **3 Results and Discussions**

101 3.1 Putting the wind event into perspective

102 By averaging the 2-meter zonal wind field over western Oregon (domain outlined in
103 Figure 1b inset, 125° - 121° W, 42° - 48° N), we plotted the daily time series of zonal wind for each
104 year including 2020 (black line; negative value indicates easterly wind). Compared with the
105 1948-2019 period, the maximum easterly occurring on 8 September 2020 wind is indeed a record
106 event. Strong easterly wind causes downslope adiabatic warming/drying that enhances fire
107 weather conditions. The fact that the 2020 record easterly wind occurred during the
108 climatologically westerly wind regime and at the height of Oregon's fire season is what made the
109 wildfires spread so rapidly. Comparison between data periods before and after 1979 also
110 suggests that the fluctuation in the day-to-day surface winds over western Oregon has increased
111 slightly. Note that actual (station) wind speeds in Oregon are greater than what the reanalysis
112 data can describe, but the data during all the 1948-2020 period in Figure 1b are consistent and so,
113 it can provide a historical perspective.

114 3.2 Diagnostic analysis

115 To analyze the stationary wave pattern evolution over the North Pacific and North
116 America, we computed the Rossby wave activity flux (WAF) using the derivation of Takaya and
117 Nakamura [2001] to depict propagating planetary waves and associated wave energy in
118 association with the mean background flow. WAF is linear and independent of time periods, so
119 we averaged the 100-300 hPa geopotential height and WAF and plotted their multi-day means,
120 from August 25-28 through September 8-12 (Figure 2b). The three typhoons are indicated in the
121 corresponding time period in which they propagated northward past 35° N while approaching
122 Korea. Snapshots of these typhoons are plotted in Figure 2c in terms of 200-hPa geopotential
123 height and 925-hPa wind vectors using GEFS initial data and, in each one, the amplified high-
124 pressure ridge to the east is patent. The Oregon extreme wind event on August 8 is shown in the
125 bottom of Figure 2c for comparison.

126 From late August through early September, the striking feature of wave amplification in
127 the geopotential height is revealed from the eastward propagating WAF across the North Pacific.
128 It takes 3-4 days for a recurving typhoon in the midlatitude to generate an amplified ridge over
129 western North America [Grams and Archambault, 2016], and Figure 2b indeed describes such a
130 feature in terms of the WAF propagation: Typhoon Bavi generated an area of significant WAF to
131 its immediate east that amplified the ridge around 150° E (8/25-28 in Figure 2b). Four days later,

132 increased WAF appeared in the Aleutian low and amplified the downstream ridge near western
133 North America (8/28-9/1). This enhanced ridge then generated its own WAF in central Canada,
134 deepening the trough there (8/31-9/4). Meanwhile, Typhoon Maysak generated new fluxes of
135 WAF that enhanced the ridge over Japan, and this further amplified the Aleutian low and the
136 downstream ridge near California. During 9/4-9/8, Typhoon Haishen repeated the process by
137 strengthening the source and propagation of WAF over the course of 5 days, making the West
138 Coast ridge and central Canada trough even stronger. We now know that this enhanced ridge
139 contributed to the California heatwave that reached its severity on September 6, followed by the
140 collapse of cold air that plowed through the intermountain West in the next two days. During
141 9/8-9/12 and after the frontal outbreak, the western North Pacific ridge weakened and so did the
142 North American wave pattern. This episode of cross-Pacific wave train was most pronounced
143 during 9/4-9/8, associated with the heatwave in California and extreme wind events in Oregon,
144 as well as record winds in Utah, where thousands of trees were uprooted, homes were destroyed
145 and at least one death (<https://www.sltrib.com/>).

146 3.3 Forecast data investigation

147 Diagnostic analysis using the WAF calculation is useful, however, it only depicts the
148 possible source and magnitude of Rossby wave dispersion. It does not identify whether the North
149 American weather that predated the historic fires would have happened without the western
150 Pacific typhoons. Moreover, atmospheric internal variability can also amplify the trans-Pacific
151 wave train without requiring external forcing like a recurving typhoon [*Orlanski and Sheldon,*
152 *1995; Schroeder et al., 2016*]. To account for these unknowns, we used the GEFS 16-day
153 forecast initialized before September to provide the closest possible scenarios of the atmospheric
154 circulation with and without the forecast typhoons.

155 For example, to investigate the effect of Typhoon Maysak's extratropical transition (e.g.,
156 00Z September 2) on the Oregon wind event (00Z September 8), we used the center value of
157 1000-hPa geopotential height (HGT_{1000}) at the typhoon's observed location to determine whether
158 the forecast captured the typhoon. Using HGT_{1000} is useful because all typhoons have a negative
159 value at their center and so, any forecast time step that shows positive value would be considered
160 a missed forecast. Typhoon Maysak on 00Z September 2, for instance, consists of various
161 forecast steps as long as 264 hours (initialized on 00Z 8/23) and as short as 78 hours (initialized
162 on 18Z 8/30). However, each typhoon also requires a different threshold of HGT_{1000} because of
163 its proximity to the forecast initial time. Our principle is to maintain balanced member sizes for
164 the "with typhoon" and "without typhoon" groups, with at least 30 members in either group. It is
165 expected that the closer the initialization is to the typhoon's presence, the more accurate GEFS
166 captures it, so the member size in the "without typhoon" group likely results from the longer
167 forecast steps (earlier forecasts). Since forecast skill is not the focus here, we did not
168 discriminate how far back or how different the initial time steps are in the composite analysis.

169 For Typhoon Bavi (6Z August 26), data up to 00Z August 26 was used to produce the
170 forecast groups based on two thresholds: 1 and 2 standard deviations of all forecasts *above* the
171 observed value of center HGT_{1000} . Forecast values less than 1 standard deviation of the ensemble
172 HGT_{1000} were considered "with typhoon" and those greater than 2 standard deviation were
173 grouped into "without typhoon". Figure 3a (inset left) shows the two groups of Typhoon Bavi
174 from the forecast and, while both groups depict a low-pressure system, the "without typhoon"

175 group (top) indicates a much weaker central pressure than the “with typhoon” group (bottom).
176 Figure 3a shows the composite 250-hPa geopotential height (HGT_{250}) on September 1 of the two
177 groups. The “with typhoon” HGT_{250} (golden contours) depicts a stronger ridge in western North
178 America accompanied by a slightly deeper trough in the upper Midwest, than the “without
179 typhoon” HGT_{250} (blue contours). We repeated the similar composite analysis using all August
180 23-30 forecast data for Typhoon Maysak based on its September 2 condition. Since Typhoon
181 Maysak was at least 54 hours away from the nearest initial forecast, we found members that
182 totally missed the typhoon. Therefore, the composite HGT_{1000} (Figure 3b inset) shows a marked
183 difference with and without the typhoon. The impact of Typhoon Maysak on September 8’s
184 HGT_{250} pattern (Figure 3b) includes an amplification of the trans-Pacific wave train all the way
185 through eastern North America, which accompanies a distinctly stronger ridge over California
186 (which is closer to observation).

187 The observed circulation pattern on September 8 was marked by a considerably more
188 undulating appearance than that with Typhoon Maysak (Figure 3b; purple dotted contours vs.
189 golden contours), likely because there was another extratropical transition by Typhoon Haishen
190 that took place a couple of days before. Figure 3c shows the HGT_{1000} composites of Typhoon
191 Haishen (00Z September 6) and associated HGT_{250} patterns on September 8. Due to the long-
192 range forecast steps of Typhoon Haishen, even the “with typhoon” composite of HGT_{1000}
193 appears weak. Nonetheless, the difference of the resultant trans-Pacific wave train between the
194 two groups is remarkable. The “with typhoon” HGT_{250} composite clearly depicts the amplified
195 wave train and phase that are in good agreement with the observed, even though by September 8
196 the forecast had approached their limit (10-16 days out). The amplified ridge-trough pattern over
197 North American was well captured, despite missing the “Z” shape over the Rocky Mountains
198 associated with the powerful frontal system. We also note that more than 60% of the members
199 that captured Typhoon Haishen also forecasted Typhoon Maysak, so the realistic wave train as
200 depicted by the “with typhoon” HGT_{250} also signifies the combined Rossby wave dispersion
201 effects from these almost back-to-back typhoons.

202 Though not shown here, we found that Typhoon Bavi alone (August 26) did not produce
203 a substantial lingering effect on the North American wave pattern after September 4. However,
204 Typhoon Bavi did contribute to the early September ridge over western North America (Figure
205 3a) leading to the buildup of hot and dry condition in West Coast, which worsened the drought
206 conditions in Oregon (<https://droughtmonitor.unl.edu/>). For verification purposes, we conducted
207 a reversed approach by using the North American wave pattern as the basis of evaluation, in
208 order to assess the difference in the forecast typhoons (see Supplemental Text). The results are
209 consistent that, for the North American wave pattern that was missed by the forecast, the prior
210 typhoon tends to be missed or underpredicted (Supplemental Figures S1-3). Conversely, when
211 the North American wave pattern was realistically depicted, the preceding typhoons were much
212 better forecasted.

213 3.4 Perspective in a changing climate

214 The analysis presented here does not have the means to address the role of climate
215 change, though it is prudent to consider climate change in the severity of these September 2020
216 extreme events. The extreme wind event in western Oregon was unprecedented but did not
217 appear to be associated with a noticeable trend. However, peripheral evidence from literature

218 may offer some clues. First, the long-term increase in aridity over western North America has
219 been reported since late 20th century [Cook *et al.*, 2004] and this trend has continued in recent
220 droughts over California and the western region [Differbaugh *et al.*, 2015; Williams *et al.*, 2015].
221 Warming and increased aridity contribute to higher risk of severe wildfires [Bryant and
222 Westerling, 2014; Dennison *et al.*, 2014; Westerling *et al.*, 2006]. Second, the observed increase
223 in the tropical ocean-atmosphere interactions that result in amplified teleconnection patterns also
224 contributed to the buildup of fuel and potential burn areas in California [Swain *et al.*, 2018; Yoon
225 *et al.*, 2015] and the western U.S. [Holden *et al.*, 2018; Voelker *et al.*, 2019]. The marked
226 amplification of the atmospheric waves over North Pacific and North America during early
227 September 2020 is in agreement with the documented change in the summertime short-wave
228 pattern along the jet stream [Kornhuber *et al.*, 2019; Mann *et al.*, 2017; Wang *et al.*, 2013].
229 Lastly, the long-term change in East Asian summer monsoon (EASM) may be relevant, given the
230 recent trend towards an enhanced EASM lifecycle consisting of the onset, break, and revival
231 phases [Wang *et al.*, 2019]. The revival phase of EASM is largely attributed to typhoon rainfall
232 and the observed poleward shift of western North Pacific tropical cyclones associated with the
233 warmer ocean [Sharmila and Walsh, 2018; Sun *et al.*, 2019] echoes the three consecutive
234 typhoons recurving and hitting Korea this year. Given the typhoon impacts on western North
235 America during a time of the year that coincides with the peak fire season, it is crucial that we
236 develop a better understanding of the extent to which the warming climate may increase the
237 extratropical transition of fall typhoons in the west Pacific.

238 Summer 2020 also saw a La Niña event developed during hurricane seasons in the
239 Northern Hemisphere (<https://www.noaa.gov/>). A developing La Niña is known to worsen the
240 southwest U.S. drought (<http://nytimes.com>) and it also modulates the western North Pacific
241 tropical cyclone activity by causing them to form in higher latitudes and recurve more easily
242 [Chen *et al.*, 2006; Han *et al.*, 2016]. Interannual variation like the ongoing La Niña cannot be
243 overlooked in future diagnostic analysis of this remarkable series of extreme events in early
244 September 2020.

245 **4 Conclusions**

246 Intrinsic meteorological variations and remote influences of atmospheric circulation are
247 demonstrated in the case of extreme events in the western U.S. in September 2020. The rapid
248 amplification of the atmospheric waves over western North America, leading to extreme heat and
249 dangerous fire weather, can be attributed to traceable effects from significant weather systems far
250 away. The succession of three recurving typhoons, which passed through the Korea Peninsula
251 within two weeks of one another, appears to have generated strong and persistent Rossby wave
252 activity to enhance the upper-tropospheric circulation—amplifying the ridge in western North
253 America and the trough in central Canada. The use of GEFS 16-day forecast and reanalysis data
254 offers an example for synoptic attribution of extreme weather events that can be done near real-
255 time. Through it, we determined the difference between possible atmospheric scenarios for
256 realistic typhoon forecasts (which went through an extratropical transition and released energy
257 into the jet stream), and “missed,” or more unrealistic, typhoon forecasts. The results portray a
258 consistent picture of Rossby wave energy being channeled through the trans-Pacific wave train
259 toward North America. If the warming ocean conditions do migrate fall typhoons poleward, as
260 suggested in the literature, then the chances of such remote influence on western North America
261 may increase. This aspect deserves further analysis.

262

263 **Acknowledgments**

264 All GEFS and reanalysis data sets are publicly available at [https://nomads.ncep.noaa.gov/
265 txt_descriptions/GFS_doc.shtml](https://nomads.ncep.noaa.gov/txt_descriptions/GFS_doc.shtml) and the authors thank the U.S. government for providing these
266 important weather data free of charges. Research fundings from the U.S. Department of
267 Energy/Office of Science under Award Number DE-SC0016605 and the SERDP project RC20-
268 3056 are acknowledged.

269

270

271 **Reference:**

- 272 Agustí-Panareda, A., S. L. Gray, G. C. Craig, and C. Thorncroft (2005), The extratropical
273 transition of Tropical Cyclone Lili (1996) and its crucial contribution to a moderate
274 extratropical development, *Monthly weather review*, 133(6), 1562-1573.
- 275 Archambault, H. M., L. F. Bosart, D. Keyser, and J. M. Cordeira (2013), A climatological
276 analysis of the extratropical flow response to recurving western North Pacific tropical
277 cyclones, *Monthly weather review*, 141(7), 2325-2346.
- 278 Bryant, B. P., and A. L. Westerling (2014), Scenarios for future wildfire risk in California: links
279 between changing demography, land use, climate, and wildfire, *Environmetrics*, n/a-n/a,
280 doi: 10.1002/env.2280.
- 281 Chen, T.-C., S.-Y. Wang, and M.-C. Yen (2006), Interannual Variation of the Tropical Cyclone
282 Activity over the Western North Pacific, *Journal of Climate*, 19(21), 5709-5720, doi:
283 doi:10.1175/JCLI3934.1.
- 284 Cook, E. R., C. A. Woodhouse, C. M. Eakin, D. M. Meko, and D. W. Stahle (2004), Long-term
285 aridity changes in the western United States, *Science*, 306(5698), 1015-1018.
- 286 Dennison, P. E., S. C. Brewer, J. D. Arnold, and M. A. Moritz (2014), Large wildfire trends in
287 the western United States, 1984–2011, *Geophysical Research Letters*, 41(8), 2928-2933.
- 288 Diffenbaugh, N. S., D. L. Swain, and D. Touma (2015), Anthropogenic warming has increased
289 drought risk in California, *Proceedings of the National Academy of Sciences*, 112(13),
290 3931-3936.
- 291 Grams, C. M., and H. M. Archambault (2016), The key role of diabatic outflow in amplifying the
292 midlatitude flow: A representative case study of weather systems surrounding western
293 North Pacific extratropical transition, *Monthly Weather Review*, 144(10), 3847-3869.
- 294 Han, R., H. Wang, Z.-Z. Hu, A. Kumar, W. Li, L. N. Long, J.-K. E. Schemm, P. Peng, W. Wang,
295 and D. Si (2016), An assessment of multimodel simulations for the variability of western
296 North Pacific tropical cyclones and its association with ENSO, *Journal of Climate*,
297 29(18), 6401-6423.
- 298 Harr, P. A., and J. M. Dea (2009), Downstream development associated with the extratropical
299 transition of tropical cyclones over the western North Pacific, *Monthly weather review*,
300 137(4), 1295-1319.
- 301 Hodyss, D., and E. Hendricks (2010), The resonant excitation of baroclinic waves by the
302 divergent circulation of recurving tropical cyclones, *Journal of the atmospheric sciences*,
303 67(11), 3600-3616.
- 304 Holden, Z. A., A. Swanson, C. H. Luce, W. M. Jolly, M. Maneta, J. W. Oyler, D. A. Warren, R.
305 Parsons, and D. Affleck (2018), Decreasing fire season precipitation increased recent

- 306 western US forest wildfire activity, *Proceedings of the National Academy of Sciences*,
307 115(36), E8349-E8357.
- 308 Jones, S. C., P. A. Harr, J. Abraham, L. F. Bosart, P. J. Bowyer, J. L. Evans, D. E. Hanley, B. N.
309 Hanstrum, R. E. Hart, and F. Lalauette (2003), The extratropical transition of tropical
310 cyclones: Forecast challenges, current understanding, and future directions, *Weather and*
311 *Forecasting*, 18(6), 1052-1092.
- 312 Kalnay, E., et al. (1996), The NCEP/NCAR 40-Year Reanalysis Project, *Bulletin of the*
313 *American Meteorological Society*, 77(3), 437-471, doi: doi:10.1175/1520-
314 0477(1996)077<0437:TNYRP>2.0.CO;2.
- 315 Kornhuber, K., S. Osprey, D. Coumou, S. Petri, V. Petoukhov, S. Rahmstorf, and L. Gray
316 (2019), Extreme weather events in early summer 2018 connected by a recurrent
317 hemispheric wave-7 pattern, *Environmental Research Letters*, 14(5), 054002.
- 318 Mann, M. E., S. Rahmstorf, K. Kornhuber, B. A. Steinman, S. K. Miller, and D. Coumou (2017),
319 Influence of Anthropogenic Climate Change on Planetary Wave Resonance and Extreme
320 Weather Events, 7, 45242, doi: 10.1038/srep45242
321 <https://www.nature.com/articles/srep45242#supplementary-information>.
- 322 Namias, J. (1963), Large-scale air-sea interactions over the North Pacific from summer 1962
323 through the subsequent winter, *Journal of Geophysical Research*, 68(22), 6171-6186.
- 324 Orlanski, I., and J. P. Sheldon (1995), Stages in the energetics of baroclinic systems, *Tellus A*,
325 47(5), 605-628.
- 326 Pantillon, F., J. P. Chaboureau, C. Lac, and P. Mascart (2013), On the role of a Rossby wave
327 train during the extratropical transition of Hurricane Helene (2006), *Quarterly Journal of*
328 *the Royal Meteorological Society*, 139(671), 370-386.
- 329 Schroeder, M., S.-Y. S. Wang, R. R. Gillies, and H.-H. Hsu (2016), Extracting the tropospheric
330 short-wave influences on subseasonal prediction of precipitation in the United States
331 using CFSv2, *Climate Dynamics*, 1-8, doi: 10.1007/s00382-016-3314-1.
- 332 Sharmila, S., and K. Walsh (2018), Recent poleward shift of tropical cyclone formation linked to
333 Hadley cell expansion, *Nature Climate Change*, 8(8), 730-736.
- 334 Sun, J., D. Wang, X. Hu, Z. Ling, and L. Wang (2019), Ongoing poleward migration of tropical
335 cyclone occurrence over the western North Pacific Ocean, *Geophysical Research Letters*,
336 46(15), 9110-9117.
- 337 Swain, D. L., B. Langenbrunner, J. D. Neelin, and A. Hall (2018), Increasing precipitation
338 volatility in twenty-first-century California, *Nature Climate Change*, 8(5), 427-433.
- 339 Takaya, K., and H. Nakamura (2001), A Formulation of a Phase-Independent Wave-Activity
340 Flux for Stationary and Migratory Quasigeostrophic Eddies on a Zonally Varying Basic
341 Flow, *Journal of the Atmospheric Sciences*, 58(6), 608-627, doi: doi:10.1175/1520-
342 0469(2001)058<0608:AFOAPI>2.0.CO;2.
- 343 Voelker, S. L., A. G. Merschel, F. C. Meinzer, D. E. Ulrich, T. A. Spies, and C. J. Still (2019),
344 Fire deficits have increased drought sensitivity in dry conifer forests: Fire frequency and
345 tree-ring carbon isotope evidence from Central Oregon, *Global change biology*, 25(4),
346 1247-1262.
- 347 Wang, S.-Y., R. E. Davies, and R. R. Gillies (2013), Identification of extreme precipitation threat
348 across midlatitude regions based on short-wave circulations, *Journal of Geophysical*
349 *Research: Atmospheres*, 118(19), 2013JD020153, doi: 10.1002/jgrd.50841.

- 350 Wang, S.-Y., H. Kim, D. Coumou, J.-H. Yoon, L. Zhao, and R. R. Gillies (2019), Consecutive
351 extreme flooding and heat wave in Japan: Are they becoming a norm?, *Atmospheric*
352 *Science Letters*, 20(10), e933, doi: 10.1002/asl.933.
- 353 Westerling, A. L., H. G. Hidalgo, D. R. Cayan, and T. W. Swetnam (2006), Warming and Earlier
354 Spring Increase Western U.S. Forest Wildfire Activity, *Science*, 313(5789), 940-943, doi:
355 10.1126/science.1128834.
- 356 Whitaker, J. S., T. M. Hamill, X. Wei, Y. Song, and Z. Toth (2008), Ensemble Data Assimilation
357 with the NCEP Global Forecast System, *Monthly Weather Review*, 136(2), 463-482, doi:
358 10.1175/2007mwr2018.1.
- 359 Williams, A. P., R. Seager, J. T. Abatzoglou, B. I. Cook, J. E. Smerdon, and E. R. Cook (2015),
360 Contribution of anthropogenic warming to California drought during 2012–2014,
361 *Geophysical Research Letters*, 42(16), 6819-6828.
- 362 Yoon, J.-H., S.-Y. S. WANG, R. R. GILLIES, L. HIPPS, B. KRAVITZ, and P. J. RASCH
363 (2015), 2. Extreme Fire Season in California: A Glimpse Into The Future?, *Bull Am*
364 *Meteorol Soc*, 96, S5-9.
- 365 Zhou, X., Y. Zhu, D. Hou, and D. Kleist (2016), A Comparison of Perturbations from an
366 Ensemble Transform and an Ensemble Kalman Filter for the NCEP Global Ensemble
367 Forecast System, *Weather and Forecasting*, 31(6), 2057-2074, doi: 10.1175/waf-d-16-
368 0109.1.
- 369

Figures 1-3.

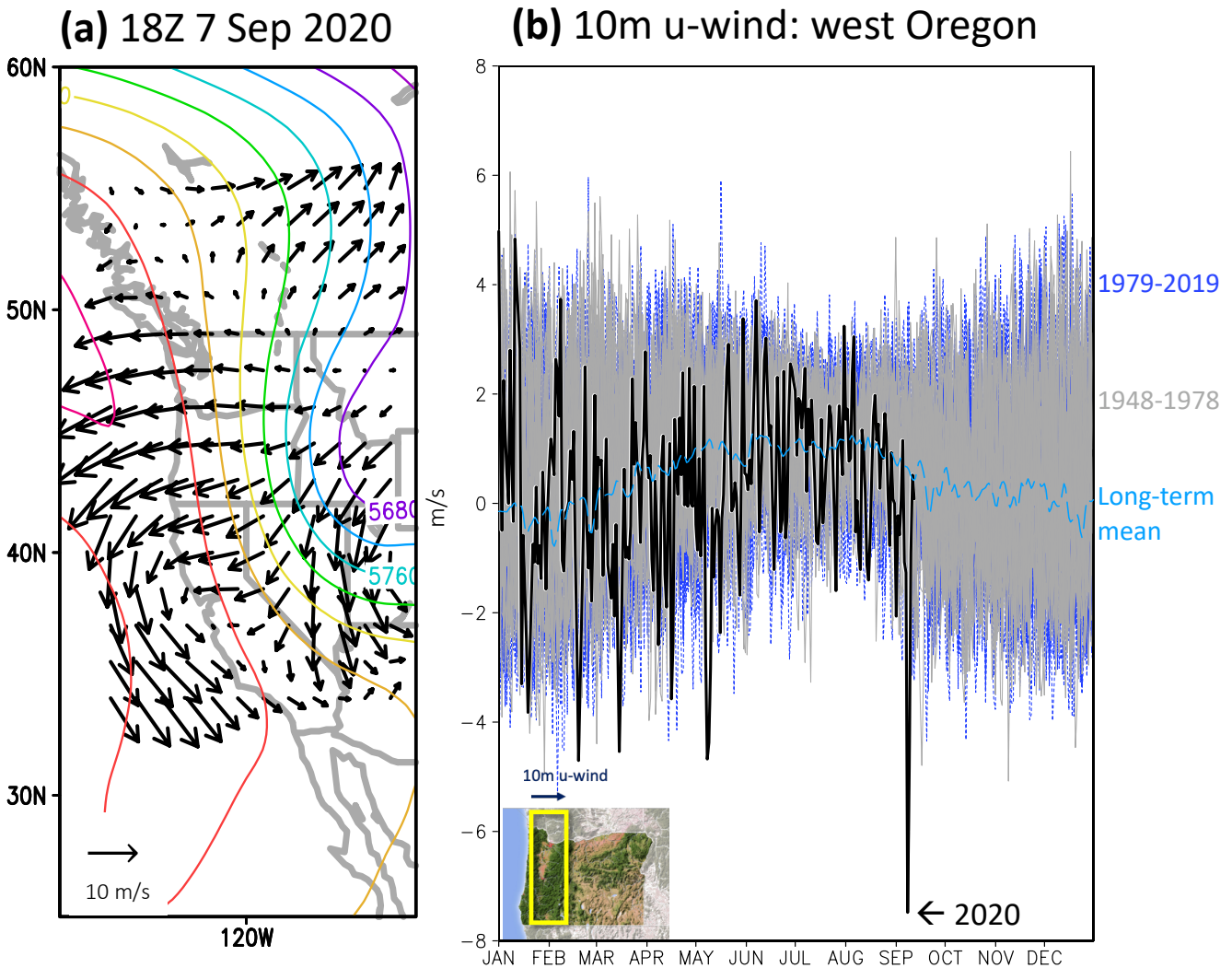
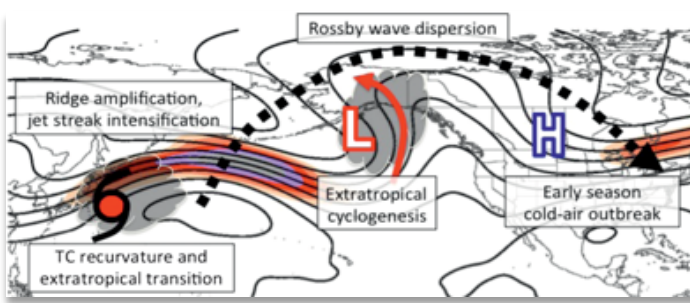
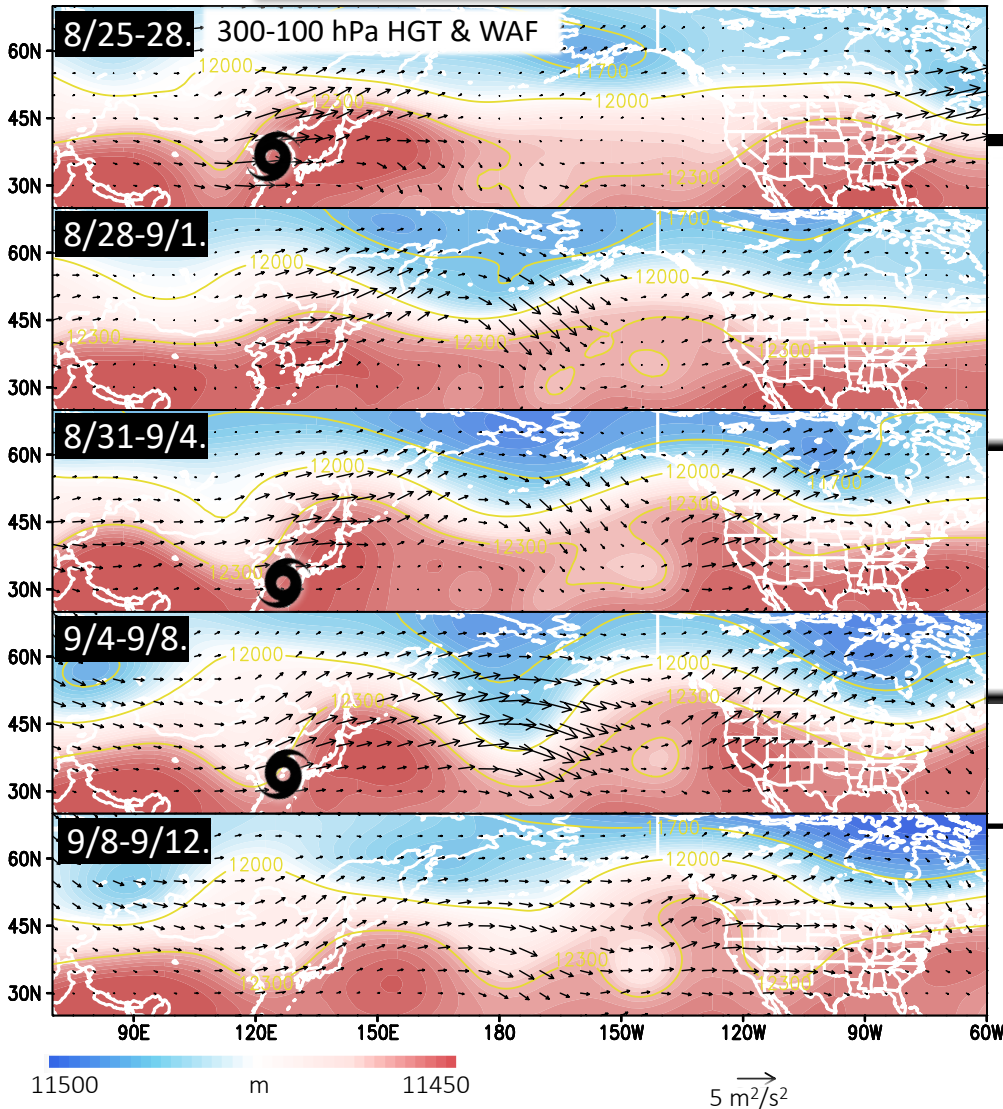
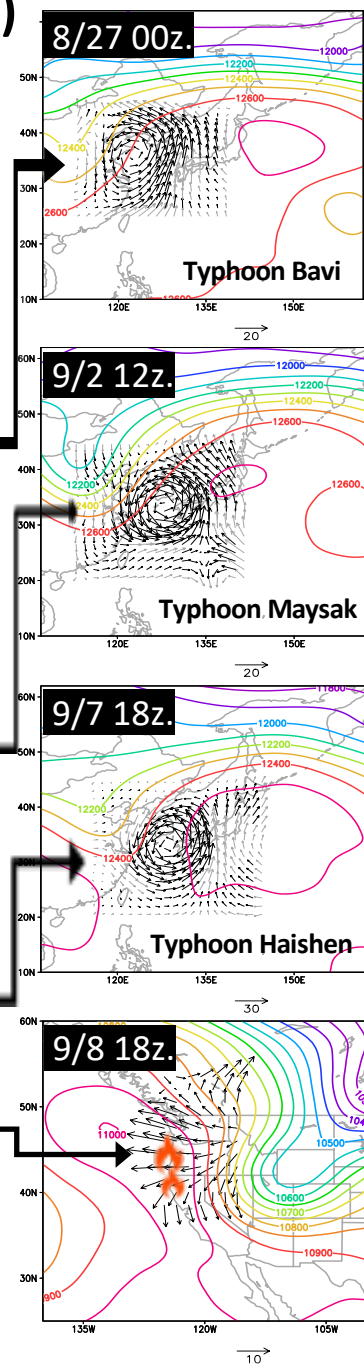


Figure 1

(a) The onset of widespread Oregon wildfires on 7 September 2020 in terms of 500-hPa geopotential height contours and 2-meter wind vectors, showing the extreme wind event at 18Z. (b) Daily time series of 10-meter zonal wind averaged over western Oregon (box area in lower-left map) in 2020 as thick black line and during 1948-1978 as gray lines and 1979-2019 as blue lines. Notice the extreme negative value indicating the record easterly wind event on 8 September 2020. The climatological zonal wind evolution is added as the light blue line.

(a)**(b)****(c)****Figure 2**

(a) Schematic diagram adopted from Archambault *et al.* [2013] depicting the process in which a recurring typhoon near Japan goes through extratropical transition and generates Rossby wave dispersion downstream, enhancing the ridge pattern in western North America. **(b)** Composites of 100-300-hPa averaged geopotential height (shadings and golden contours) and wave activity flux (vectors) over 4-5 days as indicated by the date range in upper left. Typhoon symbols indicate the extratropical transition points of the three typhoons near 130°E . **(c)** Regional depiction of each typhoons (top 3) at the time indicated in upper-left corner and typhoon name in lower right, in terms of the 250-hPa geopotential height contours and 925-hPa winds, as well as the peak wind event in West Coast (bottom, with fire symbols in western Oregon); note the different wind scales.

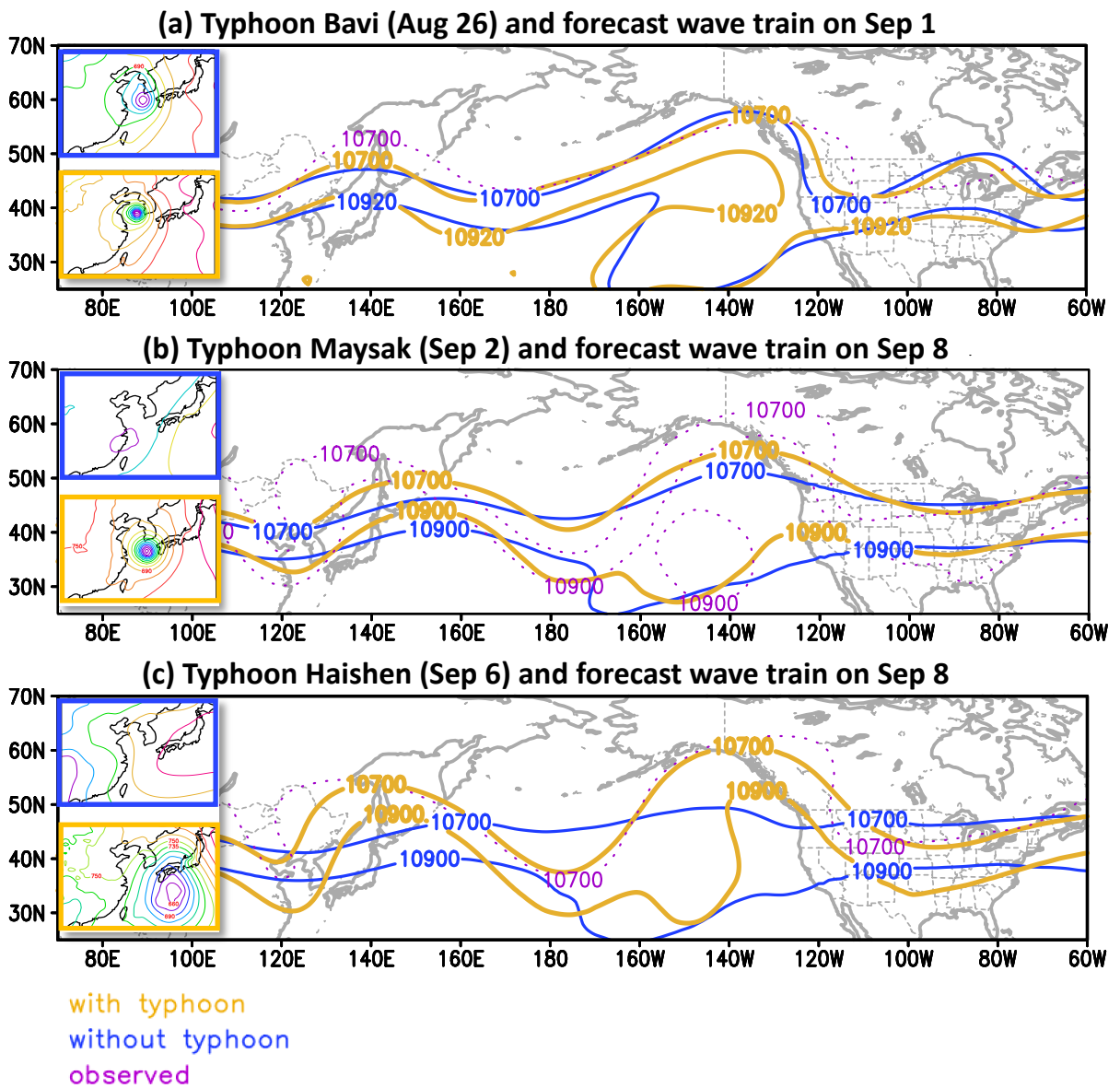


Figure 3

Composite groups of 925-hPa geopotential height for “without typhoon” (top, blue outline) and “with typhoon” (bottom, golden outline) of each forecast typhoon and the composite 250-hPa geopotential height contours in the corresponding colors, overlaid with the reanalysis height as dotted purple contour, for **(a)** Typhoon Bavi of August 26 and the wave train on September 1, **(b)** Typhoon Maysak of September 2 and the September 8 wave train, and **(c)** Typhoon Haishen of September 6 and the September 8 wave train. Note the difference in the ridge patterns over western North America and the trough patterns in the central U.S.